Published in final edited form as:

Nat Neurosci. 2011 May ; 14(5): 570–577. doi:10.1038/nn.2792.

Neuromuscular synaptic patterning requires the function of skeletal muscle dihydropyridine receptors

Fujun Chen[1], **Yun Liu**[1], **Yoshie Sugiura**[1], **Paul D. Allen**[2], **Ronald G. Gregg**[3], and **Weichun Lin**[1,†]

[1] Department of Neuroscience, UT Southwestern Medical Center, Dallas, TX 75390, USA

[2] Department of Anesthesia, Perioperative and Pain Medicine, Brigham and Women's Hospital, Boston, MA 02115, USA

[3] Department of Biochemistry and Molecular Biology, University of Louisville, Louisville, KY 40202, USA

Abstract

Developing skeletal myofibers in vertebrates are intrinsically "pre-patterned" for motor nerve innervation. However, the intrinsic factors that regulate muscle pre-patterning remain unknown. Here we show that a functional skeletal muscle dihydropyridine receptor (DHPR, the L-type Ca^{2+} channel in muscle) is required for muscle pre-patterning during the development of the neuromuscular junction (NMJ). Targeted deletion of the β1 subunit of DHPR *(Cacnb1)* in mice leads to muscle pre-patterning defects, aberrant innervation and precocious maturation of the NMJ. Reintroducing the *Cacnb1* gene into *Cacnb1*$^{-/-}$ muscles reverses the pre-patterning defects and restores normal development of the NMJ. The mechanism by which DHPRs govern muscle pre-patterning is independent of their role in excitation-contraction coupling (E-C coupling), but requires Ca^{2+} influx through the L-type Ca^{2+} channel. Our findings demonstrate that the skeletal muscle DHPR retrogradely regulates the patterning and formation of the NMJ.

The establishment of specific synaptic connections lays the foundation for neural circuitry formation. At the vertebrate NMJ, one of the best-studied model synapses, synaptogenesis occurs in a stereotypic pattern along the central regions of the post-synaptic muscle cells [1]. Emerging evidence indicates that these central regions are intrinsically pre-patterned by the muscle cells. For example, genes critical for neuromuscular synaptogenesis, including the acetylcholine receptor (*AChR)* and the muscle-specific kinase (*MuSK*), are selectively activated, and their respective proteins (AChR and MuSK) are clustered in the central regions of the muscle in the absence of innervation [2–5]. In vivo imaging in zebrafish embryos demonstrates that AChR clusters are not only pre-patterned in developing muscles

†Corresponding author: Weichun Lin, PhD, Department of Neuroscience, UT Southwestern Medical Center, 6000 Harry Hines Boulevard, Dallas, TX 75390-9111, Phone: 214-648-5935, Fax: 214-648-1801, Weichun.Lin@UTSouthwestern.edu.

Author Contributions

F. C., Y. L. and Y. S. carried the experiment, collected and analyzed the data. P.D.A. provided the RyR mutant mice. R.G.G. provided the DHPR mutant mice. W. L. supervised the project and wrote the manuscript with critical input from F.C., Y.L., Y.S., P.D.A., and R.G.G..

but also are actively incorporated into newly-formed NMJs [6,7]. Furthermore, removal of pre-patterned AChRs in mouse embryos results in excessive nerve branching and aberrant formation of the NMJ [8]. These findings challenge the long-held "neurocentric" dogma and support the opposite view that post-synaptic muscle intrinsically defines its central region for the ingrowing nerves, which subsequently fine-tune the pre-patterned AChRs so that neuromuscular synapses are generated along a narrow end-plate band of the muscle [2,9,10]. The mechanisms underlying this intrinsic pre-patterning in muscle remain unknown.

Developing myotubes generate action potentials and contract spontaneously [11], and this electrical and contractile activity is correlated with an alteration of AChR levels [12,13]. This raises the possibility that muscle electrical activity, or contractile activity, or both, are involved in pre-patterning the muscle during NMJ development. This question has been technically challenging to answer because of the difficulty in separating electrical from contractile activity, as excitation is normally coupled with contraction (E-C coupling) [14]. Most widely applied methods for manipulating activity, including tetrodotoxin (TTX), high K^+ (depolarization) or electrical stimulation, all affect both the electrical and contractile activity of the muscle. Thus, the relative contributions of electrical vs. contractile activity on neuromuscular development cannot be distinguished by applying these conventional means to perturb activity.

E-C coupling is mediated by two major membrane components – the L-type Ca^{2+} channels (DHPRs) [15], which are at the surface of the muscle membrane and act as the voltage sensor for depolarization, and the ryanodine receptors (RyRs) at the sarcoplasmic reticulum (SR), which regulate the release of Ca^{2+} from the SR into the cytosol [14]. Indeed, E-C coupling is abolished in mice deficient in either *DHPRs*, e.g. the β1 subunit of DHPR (*Cacnb1*$^{-/-}$) [16] or *RyRs* [17–19]. Therefore, we used these mutant mice (*Cacnb1*$^{-/-}$ and *RyR1*$^{-/-}$*RyR3*$^{-/-}$) to investigate the role of E-C coupling in the patterning and formation of the NMJ.

Surprisingly, muscle pre-pattern was disrupted in *Cacnb1*$^{-/-}$ muscles, but was largely preserved in *RyR1*$^{-/-}$*RyR3*$^{-/-}$ muscles. In the absence of *Cacnb1*, *AChR* and *MuSK* expression was markedly increased, leading to a broad distribution of AChR and MuSK proteins and aberrant development of the NMJ. These defects are specifically due to the loss of DHPR function in the skeletal muscle because reintroducing *Cacnb1* into *Cacnb1*$^{-/-}$ muscles genetically rescued the muscle pre-patterning defects and restored the normal patterning and formation of the NMJ. Interestingly, both electrical and synaptic activity are highly active in *Cacnb1*$^{-/-}$ muscles, suggesting the patterning defects were unlikely due to a lack of either electrical or synaptic activity. Taken together, our findings demonstrate that a functioning skeletal muscle DHPR is specifically required for establishing muscle pre-patterning during NMJ formation.

Results

A loss of DHPR function leads to abnormal synaptic patterning

Pre-patterned AChRs are clustered along the central region of the muscles at embryonic day 14.5 (E14.5); at this initial stage, the majority of the nascent AChR clusters are near, but not directly apposed to, the nerve terminals [2,4]. This is demonstrated by immunostaining of

whole mounts of E14.5 diaphragm muscles. In the WT muscle, AChR clusters were patterned to a centrally localized end-plate band (Fig. 1b) where the nerve terminals were also confined (Fig. 1d) and extended orderly branches within the central end-plate band region (Fig. 1a, g). In contrast, in *Cacnb1*$^{-/-}$ muscle, AChR clusters failed to form an end-plate band but instead were broadly distributed across the muscle, including the medial and lateral edges (Fig. 1c). For example, in the dorsal quadrant of the diaphragm muscles, AChR clusters in *Cacnb1*$^{-/-}$ mice were distributed along a length of 569 ± 10 μm (N = 5 mice) of muscle fibers, whereas AChR clusters in the control mice were confined to a length of 133 ± 6 μm (N = 5 mice) of muscle fibers. Correspondingly, the nerves in *Cacnb1*$^{-/-}$ muscles were highly branched and hyper-innervated over a broad region of the muscle, especially in the dorsal quadrant, in which the nerve branches occupied the entire muscle surface (Fig. 1e, f, h).

Because the pre-patterning is muscle intrinsic, it also occurs in aneural muscles such as the diaphragm muscle in mice deficient in the motoneuron transcription factor HB9 [2,4]. To determine whether DHPRs are required for the pre-patterning in aneural muscles, we examined the diaphragm muscles from *Cacnb1* and *HB9* double knockout mice (*Cacnb1*$^{-/-}$*HB9*$^{-/-}$). Interestingly, the muscle intrinsic, nerve-independent pre-patterning of AChR clusters in *HB9*$^{-/-}$ mice (Fig. 1i) was disrupted in *Cacnb1*$^{-/-}$*HB9*$^{-/-}$ double knockout mice. AChR clusters were found scattered over the entire muscle (Fig. 1j). Thus, like in the innervated muscle described above, DHPRs were also required for pre-patterning the aneural muscles during development.

To determine whether the pre-patterning defects displayed in the *Cacnb1*$^{-/-}$ muscles simply represent developmental delay, we examined the muscles at a later stage (E18.5). AChR clusters were confined to the central end-plate band in WT muscle (Fig. 2a) but remained scattered broadly across the entire *Cacnb1*$^{-/-}$ muscle (Fig. 2b). To determine the number of AChR clusters in individual myofibers, we dissociated E18.5 diaphragm muscles and counted them in a total of 359 control (WT or heterozygous) and 554 *Cacnb1*$^{-/-}$ myofibers. We found that multiple endplates were frequently detected in dissociated *Cacnb1*$^{-/-}$ myofibers (Fig. 2d) but rarely in control myofibers (Fig. 2c). Similar to the distribution of AChR clusters, acetylcholinesterase (AChE) was restricted to the central regions of the WT myofibers (Fig. 2h) but was broadly distributed along the entire length of the *Cacnb1*$^{-/-}$ myofibers (Fig. 2i). These findings demonstrated that the patterning defects of the *Cacnb1*$^{-/-}$ muscles persisted throughout development in *Cacnb1*$^{-/-}$ muscles, and were not attributable to developmental delay.

Both electrical and synaptic activity are detected in *Cacnb1*$^{-/-}$ muscles

Despite aberrant patterning, neuromuscular synapses were established in *Cacnb1*$^{-/-}$ muscles. As in WT (Fig. 3a–c), every end-plate in the *Cacnb1*$^{-/-}$ muscle (Fig. 3d–f) was fully innervated; that is, the pre- and post-synaptic apparatus formed in close apposition (arrows in Fig. 3c, 3f). However, individual synapses appeared larger in the *Cacnb1*$^{-/-}$ muscle, compared to the age-matched controls. We therefore measured the sizes of individual end-plates and found a two-fold increase in size of end-plates in the *Cacnb1*$^{-/-}$ muscles, compared to the controls (supplementary Fig. S1). Additionally, 99.4% (n=342) of

the end-plates in the control myofibers retained an oval shape (Fig. 3b) that is characteristic of embryonic end-plates [20]. In contrast, nearly half (48.6%, n=399) of the end-plates in *Cacnb1*$^{-/-}$ muscles appeared to be perforated (arrowheads, Fig. 3e), which was an indication that the end-plates were more matured than those in the WT muscles [20]. Thus, the post-synaptic end-plates in *Cacnb1*$^{-/-}$ muscles appeared precociously matured, compared with those in the age-matched WT muscles, suggesting that muscle DHPR activity may negatively regulate the maturation of the NMJ during development.

To further examine neuromuscular synapses, we carried out electron microscopy analyses. We found that the *Cacnb1*$^{-/-}$ muscle were markedly thinner and the sarcomeres were less well aligned compared with the control muscles (supplementary Fig. S2). However, the pre-synaptic nerve terminals in *Cacnb1*$^{-/-}$ mice contained abundant synaptic vesicles and well-defined basal lamina (arrow in Fig.3h).

To determine if the neuromuscular synapses in the *Cacnb1*$^{-/-}$ mice were functional we performed electrophysiological analysis. We found that neuromuscular synaptic activity in *Cacnb1*$^{-/-}$ mice was markedly increased compared to their littermate controls. For example, mEPP frequency (events/minute) was increased more than 60-fold in *Cacnb1*$^{-/-}$ muscles (57.86 ± 12.73, n = 38 cells, N = 4 mice, 8635 total events in 181 minutes), compared with controls (0.85 ± 0.16, n = 26 cells, N = 4 mice, 104 total events in 128 minutes) (P = 0.00007). Furthermore, spontaneous action potentials were more frequently detected in *Cacnb1*$^{-/-}$ muscle cells (58%, or 22/38 muscle cells) (Fig. 3l) compared with control muscle cells (8%, or 2/26 muscle cells) (Fig. 3k). In addition, mEPP amplitudes were also significantly increased in *Cacnb1*$^{-/-}$ mice (3.19 ± 0.22 mV, n=38 cells, N=4 mice), compared with the control (2.57 ± 0.19 mV, n=26 cells, N=4 mice) ($P < 0.0047$). Interestingly, EPP amplitudes were similar between control (13.25 ± 1.25 mV, n = 23 cells, N = 4 mice) and *Cacnb1*$^{-/-}$ mice (12.75 ± 1.22 mV, n = 27 cells, N = 4 mice) (P = 0.227), and action potentials were elicited in both control and *Cacnb1*$^{-/-}$ muscles in response to electrical stimulation of the nerve. Together, these results demonstrated that both the electrical and synaptic activity were highly active in the *Cacnb1*$^{-/-}$ muscles. Thus, the abnormal patterning of the NMJ that was displayed in *Cacnb1*$^{-/-}$ muscles cannot be attributed to a lack of electrical or synaptic activity in these muscles.

Muscle-specific expression of *Cacnb1* rescues the patterning defects in *Cacnb1*$^{-/-}$ muscle

Since Cacnb1 is expressed in both skeletal muscles and neurons [21], we considered the possibility that the lack of Cacnb1 in neurons might have contributed to the defects of the NMJ in *Cacnb1*$^{-/-}$ mice. We therefore examined compound mutant mice specifically lacking *Cacnb1* expression in neurons [22]. These compound mutant mice were generated based upon previous studies demonstrating that reintroducing *Cacnb1* cDNA into *Cacnb1*$^{-/-}$ myotubes completely restores Ca^{2+} current, charge movements and Ca^{2+} transients to normal levels [23] and that human skeletal actin (HSA) promoter-driven *Cacnb1* (HSA::*Cacnb1*) restores *Cacnb1* expression specifically in *Cacnb1*$^{-/-}$ skeletal muscles. These compound mutant mice (*HSA::Cacnb1; Cacnb1*$^{-/-}$, hereafter referred to as the rescued mice) are normal, viable and express *Cacnb1* in skeletal muscles but not in neurons [22].

We found that the levels of synaptic activity and the patterns of the neuromuscular synapses were restored to normal in the rescued mice (Fig.4): the level of neuromuscular synaptic activity was similar between the control (Fig. 4a) and the rescued mice (Fig. 4b). For example, mEPP frequency was restored to normal in the rescued mice (*Cacnb1*$^{-/-}$*; HSA::Cacnb1*, 1.07±0.10, n=53 cells, N=7 mice) compared with the control (1.00±0.09, n=47 cells, N=5 mice). The mEPP amplitudes (control, 2.00±0.08 mV, n=51 cells, N=5 mice; rescue, 1.92±0.06 mV, n=65 cells, N=7 mice) and EPP amplitudes were also similar between control and rescued mice (control: 15.56±0.61 mV, n=61 cells, N=5 mice; rescue: 14.07±0.60 mV, n=72 cells, N=7 mice).

Likewise, the patterning of the NMJs was also restored to normal in the rescued mice (Fig. 4c–h), similar to that displayed in the WT mice (Fig. 1b, d, g, Fig. 2f). Since the rescued mice were viable, we further followed their NMJ development to postnatal stages. We found that postnatal NMJ patterns and sizes of the individual end-plates were also restored to normal in the rescued mice (Supplementary Fig. S3). Furthermore, AChE expression patterns in the rescued mice (Fig. 4k–l) were indistinguishable from those of control mice (Fig. 4i–j). These results demonstrated that muscle-specific expression of *Cacnb1* was sufficient to rescue the patterning defects of the NMJ in *Cacnb1*$^{-/-}$ mice, and that the muscle DHPR, but not the neuronal DHPR was required for the establishment of the normal pattern of the NMJ.

Distinct phenotype in pre-patterning between *Cacnb1*$^{-/-}$ and *RyR1*$^{-/-}$*RyR3*$^{-/-}$ muscles

DHPRs directly interact with and activate the RyRs and initiate E-C coupling. To determine whether the defects of muscle pre-patterning in the *Cacnb1*$^{-/-}$ mice had resulted from a disruption of E-C coupling, we examined mutant mice deficient in RyRs, which were thus lacking E-C coupling. Mice have three distinct *RyR* genes, *RyR1*, *RyR2* and *RyR3* [24]. Because both RyR1 and RyR3 are expressed in embryonic skeletal muscles [25], we therefore focused on double mutant mice deficient in both *RyR1* and *RyR3* (*RyR1*$^{-/-}$*RyR3*$^{-/-}$) [19].

Surprisingly, unlike the *Cacnb1*$^{-/-}$ muscles in which AChR clusters were broadly distributed (Fig. 1c), AChR clusters were confined to the central region in E14.5 *RyR1*$^{-/-}$*RyR3*$^{-/-}$ muscle (Fig. 5d). The average width of the endplate band in *RyR1*$^{-/-}$*RyR3*$^{-/-}$ muscles, however, was increased compared to E14.5 WT muscles. For example, in the dorsal quadrant of the diaphragm muscles, the average width of the end-plate band was 154 ± 13 μm in *RyR1*$^{-/-}$*RyR3*$^{-/-}$ mice (N = 5 mice) and 133 ± 6 μm (N = 5 mice) in WT mice. Importantly, a central end-plate band was present in E14.5 *RyR1*$^{-/-}$*RyR3*$^{-/-}$ muscles, indicating that the muscle pre-pattern was established in E14.5 *RyR1*$^{-/-}$*RyR3*$^{-/-}$ muscles. Interestingly, innervation in the *RyR1*$^{-/-}$*RyR3*$^{-/-}$ muscle (Fig. 5e) was markedly increased compared with the littermate control (*RyR*$^{+/+}$*RyR3*$^{+/-}$) (Fig. 5b). Nevertheless, the nerve terminals in the *RyR1*$^{-/-}$*RyR3*$^{-/-}$ muscle were confined to the central end-plate band (Fig. 5f), distinctly different from that was seen in the *Cacnb1*$^{-/-}$ muscles (Fig. 1e, h). As development proceeded to a later stage (E18.5), numerous ectopic AChR clusters appeared in the peripheral regions of the *RyR1*$^{-/-}$*RyR3*$^{-/-}$ muscle, but the majority of AChR clusters were still aligned to a centrally localized endplate band (Fig. 5h), in a pattern different from that seen in the *Cacnb1*$^{-/-}$ muscle (Fig. 5i). These data suggest

that the pre-patterning defects in the *Cacnb1*$^{-/-}$ muscle are specifically attributed to the loss of functioning DHPRs, but neither to the lack of muscle contractile activity nor to the absence of SR Ca^{2+} release resulting from the loss of the RyRs.

Skeletal muscle DHPRs regulate the expression of *AChR* and *MuSK*

During normal neuromuscular development, AChR genes are selectively transcribed at myonuclei near the synaptic sites (sub-synaptic myonuclei) and suppressed at extra-synaptic myonuclei; as a result, *AChR* transcripts are localized at the central end-plate band [26]. This specific pattern of *AChR* expression is also pre-patterned in the muscle, as it is maintained in the absence of innervation [2,4]. We therefore examined the levels and patterns of AChR gene expression in *Cacnb1*$^{-/-}$ muscles. Using quantitative real-time RT-PCR, we found that *AChR*α-subunit (*AChRα*) expression was significantly increased in E14.5 *Cacnb1*$^{-/-}$ muscles compared with WT muscles (relative expression levels of *AChR*α: WT, 1.00 ± 0.20, N= 8 mice; *Cacnb1*$^{-/-}$, 2.82 ± 0.25, N= 8 mice; $P = 0.007$). In addition, in situ hybridization revealed that the pattern of *AChRα* expression in the E14.5 *Cacnb1*$^{-/-}$ diaphragm muscle was completely disrupted, being broadly distributed along the entire surface (Fig. 6b), rather than being localized to the central region, as in the E14.5 WT diaphragm muscle (Fig. 6a). Similar to the disruption of the AChR clustering, the disruption of *AChRα* expression pattern persisted throughout development. For example, *AChRα* transcripts were detected only in the central regions of the E18.5 WT intercostal muscles (Fig. 6c, left panel), but were uniformly distributed in the E18.5 *Cacnb1*$^{-/-}$ intercostal muscles (Fig. 6c, middle panel). The normal pattern of *AChRα* expression was restored in the intercostal muscles of the rescued mice (*HSA::Cacnb1; Cacnb1*$^{-/-}$) (Fig. 6c, right panel).

How does DHPR function to pre-pattern the developing myofibers? Because the muscle specific kinase, MuSK, is expressed in the central regions of the muscle, independent of innervation, and overexpressing *MuSK* leads to a broadening of end-plate bands and innervation zones [5], we hypothesized that the patterning defects of *Cacnb1*$^{-/-}$ muscles may be due to altered expression of *MuSK*. We therefore measured *MuSK* expression levels in *Cacnb1*$^{-/-}$ muscles and found that *MuSK* expression was significantly increased in E14.5 *Cacnb1*$^{-/-}$ muscles compared with E14.5 WT muscles (relative expression levels of *MuSK*: WT, 1.00 ± 0.23, N= 8 mice; *Cacnb1*$^{-/-}$, 2.12 ± 0.21, N= 8 mice; $P = 0.006$). Furthermore, *MuSK* transcripts were broadly distributed along the entire *Cacnb1*$^{-/-}$ muscle (Fig. 6d, right panel) rather than being concentrated at the central end-plate band as they were in WT muscles (Fig. 6d, left panel). To examine the distribution of MuSK protein, we double-labeled diaphragm muscles with anti-MuSK antibody and α-bungarotoxin. We found that the MuSK protein was detected throughout the *Cacnb1*$^{-/-}$ muscle, coinciding with the broad distribution pattern of AChR clusters in the *Cacnb1*$^{-/-}$ muscle (Fig. 6f, middle panels), whereas MuSK protein was detected along the central region of the muscle in the WT (Fig. 6f, left panels). Like the AChR pattern, the normal distribution pattern of MuSK protein was also restored in the rescued mice (Fig. 6f, right panels). These findings demonstrated that functional DHPRs were necessary for regulating both the level and the pattern of MuSK expression.

To further elucidate the mechanisms by which DHPRs regulate the expression of *AChR* and *MuSK*, we tested whehter Ca^{2+} influx through the L-type channels was involved. We treated WT myotube cultures (C2C12) [27] with L-type Ca^{2+} channel antagonists, including verapamil and isradipine [28]. We found that both verapamil and isradipine significantly increased the relative expression levels of *MuSK* and *AChR* compared with controls. Conversely, the L-type Ca^{2+} channel agonist (Bay K 8644) significantly decreased the expression of *AChR* and *MuSK* compared with controls (Fig. 6e). Together, these results demonstrated that muscle DHPRs regulate the expression of *AChR* and *MuSK* through Ca^{2+} influx.

Discussion

Using genetic approaches in mice, we have revealed an unexpected role of the DHPRs in the establishment of muscle pre-patterning during neuromuscular synaptogenesis. We found that DHPR function is necessary for regulating proper levels and patterns of *AChR* and *MuSK* expression. In the absence of muscle DHPR function, *AChR* and *MuSK* expression is up regulated and AChR and MuSK protein is broadly distributed, resulting in pre-patterning defects. We further demonstrated that DHPRs regulate the expression of *AChR* and *MuSK* through Ca^{2+} influx, because application of L-type Ca^{2+} channel antagonists to WT myotubes increased the expression of *AChR* and *MuSK*, whereas application of L-type Ca^{2+} channel agonists decreased their expression (summarized in Supplementary Fig. S4).

The mechanism by which DHPRs govern muscle pre-patterning is likely independent of their roles in E-C coupling, as distinct phenotype in AChR clustering is displayed between *Cacnb1*$^{-/-}$ and *RyR1*$^{-/-}$*RyR3*$^{-/-}$ muscles, which both lack E-C coupling. These findings indicate that DHPRs are the major contributors for regulating the establishment of muscle pre-patterning. This is further supported by our genetic rescue experiments that restore the normal muscle pre-pattern when *Cacnb1* is specifically reintroduced into *Cacnb1*$^{-/-}$ muscles.

Interestingly, at a later stage (E18.5) of development, numerous AChR clusters appear ectopically outside of the central end-plate band in *RyR1*$^{-/-}$*RyR3*$^{-/-}$ muscles. These results indicate that RyRs, although not being required for the establishment of muscle pre-patterning at the initial stage of neuromuscular synaptogenesis (E14.5), are important for the subsequent development of the NMJ. In addition, like *Cacnb1*$^{-/-}$ muscles, innervation is markedly increased in *RyR1*$^{-/-}$*RyR3*$^{-/-}$ muscles. One possible contributing factor for the emergence of ectopic AChR clusters in E18.5 *RyR1*$^{-/-}$*RyR3*$^{-/-}$ muscles and the resemblance of increased innervation between *Cacnb1* and *RyR* null muscles is that the L-type Ca^{2+} current is significantly reduced, although not completely eliminated, in *RyR* null muscles [18,29]. Alternatively, increased innervation in both *Cacnb1* and *RyR* null muscles could be attributed to an enhanced motoneuron survival resulted from a blockade of muscle contractile activity in these mutant muscles; the underlying mechanism remains to be further elucidated.

One of the most intriguing findings from previous studies is that aneural muscles in *HB9*$^{-/-}$ mice are capable of pre-patterning the expression of AChR [2,4] and MuSK [5] in the absence of

the nerves. Our present study demonstrates that the pre-patterning of aneural muscle in *HB9*$^{-/-}$ mice requires DHPR function, because *HB9*$^{-/-}$ *Cacnb1*$^{-/-}$ double knockout mice fail to establish muscle pre-patterning. This finding provides an important step for elucidating mechanisms underlying muscle intrinsic pre-patterning. Muscle fibers depolarize spontaneously during development [11]. Membrane depolarization is detected by the DHPR, which functions both as a voltage sensor and a L-type Ca^{2+} channel and initiates Ca^{2+} influx [14]. This depolarization-initiated Ca^{2+} influx through the DHPR negatively regulates *AChR* and *MuSK* expression. In the absence of Cacnb1, L-type Ca^{2+} currents are absent [16,30], this negative regulation is lost, allowing increased *AChR* and *MuSK* expression and a disruption of muscle pre-patterning.

In addition to their predominant localization in the transverse tubular membrane, DHPRs are also found in discrete foci in the sub-sarcolemmal region of the muscle [31], raising the possibility that DHPRs may directly regulate gene expression independent of their roles in regulating Ca^{2+} channel activity. Indeed, previous studies have shown that the C terminus of the L-type Ca^{2+} channels in cardiac muscles functions as a transcription factor and directly regulates gene transcription [32,33]. Additionally, the Ca^{2+} channel β_3 subunit, a homolog of *Cacnb1*, regulates gene transcription by interacting with a novel isoform of Pax6 [34]. These studies suggest a possibility that Cacnb1 (DHPR β1) may also exert its effect on gene expression, like DHPR β_3 does, by functioning directly as a transcription factor or by binding to one or more novel transcription factor. However, our data demonstrate that the underlying mechanism that leads to an increase in *AChR* and *MuSK* expression in *Cacnb1*$^{-/-}$ muscles is attributed to the loss of L-type Ca^{2+} channel activity, because application of L-type Ca^{2+} channel agonist and antagonists in WT muscles lead to a significant decrease and increase, respectively, of both *AChR* and *MuSK* expression.

The abnormal innervation defects displayed in *Cacnb1*$^{-/-}$ muscles resemble those reported in mice with muscular dysgenesis (*mdg*) [35–37], a lethal autosomal recessive mutation leading to an absence of the α_{1s} subunit of DHPR [38]. It was proposed that the defects seen in *mdg* mice are “neurogenic” rather than “myogenic” in nature, based on experiments in which *mdg* muscles that were co-cultured with normal spinal cord neurons were thought to regain normal muscle activity [39,40]. Our transgenic rescue experiment unequivocally demonstrates that the defects of abnormal NMJ development in *Cacnb1*$^{-/-}$ mice are myogenic, i.e., the result of a lack of muscle DHPR function, with no effect exerted by neuronal DHPRs.

Previous studies have demonstrated that electrical activity plays crucial roles in regulating neuromuscular synapse formation during development and regeneration. For example, blocking electrical activity increases *AChR* [26,41,42] and *MuSK* [43] expression in the skeletal muscles. Conversely, enhancing electrical activity suppresses *AChR* expression in skeletal muscles [44]. Recent studies have further indicated that the activity-dependent gene expression is regulated by histone deacetylases (HDACs), such as *HDAC9* [45], or *HDAC4* [46]. Because muscle electrical activity is not only present but also significantly enhanced in *Cacnb1*$^{-/-}$ muscles, one would expect *AChR* and *MuSK* expression in *Cacnb1*$^{-/-}$ muscles to be suppressed. To the contrary, we found that *AChR* and *MuSK* expression are significantly increased and that *AChR* and *MuSK* transcripts are broadly distributed along the *Cacnb1*$^{-/-}$ muscle. These results suggest that the mechanism by which electrical activity suppresses

AChR and *MuSK* expression is that it must activate the muscle DHPRs, the L-type Ca^{2+} channel in skeletal muscles. Interestingly, a previous study has shown that L-type Ca^{2+} channel activity regulates the metabolic stabilization of end-plate AChRs in chronically denervated soleus muscles in adult rats [47]. Furthermore, L-type channels are also involved in regulating neuronal gene transcription [48,49]. Therefore, L-type Ca^{2+} channel activity is likely one of the common mechanisms underlying activity-dependent gene expression in various types of excitable cells including nerve and muscle cells.

Online Methods

Mice

Mutant mice deficient in the DHPR β_1 subunit (MGI: 2181804, *Cacnb1*^{tm1Rgg}, or *Cacnb1*) [16], *RyR1RyR3* [19] and *HAS::Cacnb1* transgenic mice [22] have been described previously. *HB9* mutant mice [50] were obtained from the Jackson Lab (stock number 006600, strain name: B6.129S1-*Mnx1*$^{tm4(cre)Tmj}$/J). Homozygous null (*Cacnb1*$^{-/-}$, *HB9*$^{-/-}$ and *RyR1*$^{-/-}$*RyR3*$^{-/-}$) or rescued *Cacnb1*$^{-/-}$ mutants (*Cacnb1*$^{-/-}$; *HAS::Cacnb1)* were obtained by dated pregnancies of heterozygous mating; the day when a vaginal plug first appeared was designated as embryonic (E) day 0.5. After selected intervals of development, null embryos and their littermate controls [including wild-type (WT, +/+) and heterozygous (+/−)] were collected by Cesarean section of anesthetized pregnant mice. All experimental protocols followed NIH Guidelines and were approved bythe UT Southwestern Institutional Animal Care and Use Committee.

Light and electron microscopic analysis of the NMJ

Immunofluorescence labeling of the embryonic NMJs was performed as described [8]. Whole mounts of diaphragm and intercostal muscles were fixed in 2% paraformaldehyde (PFA) in 0.1 M phosphate buffer (pH 7.3) overnight at 4°C. The samples were blocked in dilution buffer (500 mM NaCl, 0.01 M phosphate buffer, 3% BSA and 0.01% thimerosal), and then incubated overnight at 4°C with anti-neurofilament 150 (NF150) plus anti-synaptotagmin-2 (Syt 2) antibodies, or with anti-MuSK antibodies. After extensive washes, muscle whole mounts were then incubated with fluorescein isothiocyanate (FITC)-conjugated secondary antibody and Texas Red-conjugated α-bungarotoxin (α-bgt) (10^{-8} M, Invitrogen Corporation, Carlsbad, CA). Samples were then washed with PBS and mounted in VECTASHIELD mounting medium (Vector Laboratories, Inc. Burlingame, CA). Images were acquired using a Zeiss LSM 510 Meta confocal microscope. Acetylcholinesterase (AChE) staining was carried out in whole mounts of diaphragm or triangularis sterni muscles. Muscles were fixed with 2% PFA in 0.1 M phosphate buffer (pH 7.3) overnight at 4°C. After extensive wash in PBS, the muscles were pre-incubated at 37 °C for 1 hr in a solution (pH 5.5) containing ethopropazine (0.2 mM), acetylthiocholine iodine (4 mM), glycine (10 mM), cupric sulfate (2 mM) and sodium acetate (65 mM). The muscle samples were then incubated at room temperature and under a fume hood for 2–5 minutes in sodium sulfide (1.25%, pH 6.0), followed by extensive wash in water (under a fume hood). The muscles were then flat mounted onto a glass slide and imaged under a stereomicroscope (SteREO Discovery V8, Carl Zeiss).

Quantification of endplates (AChR patches) in dissociated single myofibers was carried out in E18.5 diaphragm muscles isolated from 3 pairs of control (WT or heterozygous) and *Cacnb1*$^{-/-}$ mice. The diaphragms were digested with 0.2% of collagenase in Dulbecco's Modified Eagle's Medium (DMEM) at 37°C for 30 minutes, fixed in 1% PFA for 15 min on ice, washed in PBS and stained with FITC-conjugated α-bungarotoxin (10^{-8} M, Invitrogen Corporation, Carlsbad, CA) to label endplates and Rhodamine conjugated phalloidin (1:200, Invitrogen Corporation, Carlsbad, CA) to label myofibers. Images were acquired using a Zeiss LSM 510 Meta confocal microscope.

For electron microscopy, E18.5 diaphragm and intercostal muscles were immersion-fixed in freshly prepared 1% glutaraldehyde plus 4% PFA in 0.1-M phosphate buffer (pH 7.4). Tissues were then dissected and remained in the same fixative overnight. The tissues were post-fixed with 1% osmium tetroxide and embedded in Epon 812. Ultrathin-sections (70–80 nm) were stained with uranyl acetate and lead citrate, and observed using a Tecnai transmission electron microscope.

Electrophysiology

Electrophysiological analyses were carried out as previously described [8]. Briefly, phrenic nerve-diaphragm muscles (E18.5 or P0) were dissected in oxygenated (95% O_2 and 5% CO_2) rodent normal Ringer's solution (NaCl 136.8mM, KCl 5mM, $MgCl_2$ 1mM, NaH_2PO_4 1mM, $NaHCO_3$ 12 mM, D-Glucose 11mM, $CaCl_2$ 2mM). The preparation was left in the oxygenated Ringer's solution for at least 30 minutes before recording. All the recordings were performed at room temperature (22°C). The end-plate region was impaled by a glass micropipette (30–40 MΩ) filled with solution containing 2 M potassium citrate and 10 mM KCl. A square-pulse stimulation (0.1ms, 2V) was delivered to the nerve via a suction electrode connected to an external stimulator (Model: SD9, Grass, USA). The signal was amplified by an AxonClamp-2B amplifier (Molecular Devices, USA) and digitized at 10kHz by Digidata 1322A (Molecular Devices, USA). Data were recorded by Clampex software (Molecular Devices, USA) and stored in a PC for further off-line analysis.

Myotube culture

Mouse C2C12 cells [27] were obtained from American Type Culture Collection (ATCC, Manassas, VA). Cells were plated in 60 mm culture dishes coated with 1% gelatin overnight. Cells (myoblasts) were initially cultured in Dulbecco's modified Eagle's medium (DMEM) (Gibco, GlutaMAX) with 20% fetal bovine serum and 0.5% chick embryo extract, without antibiotics, at 37 °C, 8% CO_2. Upon reaching 90% confluence, the culture medium was replaced with DMEM plus 2% horse serum to induce myotube fusion. After an additional 72 hours, myotube cultures were treated with either the L-type Ca^{2+} channel antagonists including isradipine (1 μM) for 48 hours or verapamil (10 μM) for 24 hours, or treated with the L-type Ca^{2+} channel agonist (S)-(−)- Bay K 8644 (10 μM) for 24 hours. Vehicle controls include DMSO or medium only. To maximize the uniformity in drug treatment, all reagents were freshly prepared and were mixed gently with culture medium prior to application to the cultures. Both L-type Ca^{2+} channel antagonists (isradipine and verapamil) and agonist (S)-(−)-Bay K 8644 were purchased from Tocris Bioscience (Ellisville, MO).

RT-PCR and quantitative real-time PCR

Total RNAs were isolated from E14.5 hindlimbs of mouse embryos, or from C2C12 myotube cultures using TRI reagent (Molecular Research Center, Cincinnati, OH). First-strand cDNAs were synthesized using SuperScript III cDNA synthesis kit (Invitrogen Corporation, Carlsbad, CA). Quantitative real-time PCR was performed by using Fast SYBR Green Master Mix on a 7500 Fast Real-Time PCR System (Applied Biosystems, Foster City, CA). Each sample was assayed in triplicate reactions. The amplificationdifference between *AChR α-subunit* and *muscle creatine kinase (Mck)*, or between *MuSK* and *Mck* in each sample was calculated and then normalized to that of wild-type muscles or control myotube cultures using the comparative C_T method (Applied Biosystems, Foster City, CA). The following primers were used for PCR amplification of specific gene products: (1) *AChR α-subunit* - forward AAG CTA CTG TGA GAT CAT CGT CAC, reverse TGA CGA AGT GGT AGG TGA TGT CCA; (2). *MuSK* -forward CCC TGC AAG TGA AGA TGA AA, reverse TTC AAG AAC TGC GAT TCT GG; (3). *Mck* – forward CGT GTC ACC TCT GCT GCT, reverse CCT TCA TAT TGC CTC CCT TCT [5].

Statistical Analysis

The Student's *t*-test was applied to assess statistical differences. Differences were considered statistically significant if the p-value (*P*) was less than 0.05. All quantitative data were presented as means ± standard error of the mean (SEM).

In situ hybridization

Whole mount in situ hybridization was carried out as previously described [2]. Briefly, ribcages including diaphragm and intercostal muscles were fixed in freshly prepared 4% PFA in 0.1 M phosphate buffer at 4°C overnight and then dehydrated through a series of methanol solutions (25, 50, 75 and 100%). Hybridization was carried out at 70°C overnight in hybridization buffer containing 50% formamide, 1.3X SSC, 50 μg/ml yeast tRNA, 0.2% Tween-20, and 1% Triton X-100, using digoxigenin-labeled *α-AChR* [26] or *MuSK* [5] riboprobes. After hybridization, the samples were washed with TBS containing 1% Tween-20, blocked with 5% goat serum in dilution buffer, and incubated with alkaline phosphatase conjugated anti-digoxigenin (1:1000, Boehringer Mannheim) overnight at 4°C, and hybridization signals were detected in a staining solution containing 100 mM Tris (pH 9.5), 0.4 mg/ml nitro blue tetrazolium chloride (NBT), 0.19 mg/ml 5-Bromo-4-chloro-3-indolyl phosphate (BCIP), 100mM NaCl and 50 mM $MgCl_2$.

Supplementary Material

Refer to Web version on PubMed Central for supplementary material.

Acknowledgments

We thank Drs. Joseph Takahashi, Eric Olson, Ben Szaro, Jane Johnson, Carla Green, Keith Walton, Jonathan Terman, Joseph McArdle and Rhonda Bassel-Duby for critical reading and commenting on the manuscript, Steve Cannon, David Francis, Ege Kavalali and Ilya Bezprozvanny for valuable suggestions on muscle physiology, and Steven Burden for AChRα and MuSK in situ probes. This study was supported by grants (to W. Lin) from the NIH/NINDS (NS 055028), from the Edward Mallinckrodt, Jr. Scholar Program, and from the Cain Foundation in

Medical Research at UT Southwestern Medical Center and by a grant (to P. Allen) from the NIH/NIAMS (P01AR044750).

References

1. Hall ZW, Sanes JR. Synaptic structure and development: the neuromuscular junction. Cell. 1993; 72 (Suppl):99–121. [PubMed: 8428377]
2. Lin W, et al. Distinct roles of nerve and muscle in postsynaptic differentiation of the neuromuscular synapse. Nature. 2001; 410:1057–64. [PubMed: 11323662]
3. Yang X, Li W, Prescott ED, Burden SJ, Wang JC. DNA topoisomerase IIbeta and neural development. Science. 2000; 287:131–4. [PubMed: 10615047]
4. Yang X, et al. Patterning of muscle acetylcholine receptor gene expression in the absence of motor innervation. Neuron. 2001; 30:399–410. [PubMed: 11395002]
5. Kim N, Burden SJ. MuSK controls where motor axons grow and form synapses. Nat Neurosci. 2008; 11:19–27. [PubMed: 18084289]
6. Flanagan-Steet H, Fox MA, Meyer D, Sanes JR. Neuromuscular synapses can form in vivo by incorporation of initially aneural postsynaptic specializations. Development. 2005; 132:4471–81. [PubMed: 16162647]
7. Panzer JA, Song Y, Balice-Gordon RJ. In vivo imaging of preferential motor axon outgrowth to and synaptogenesis at prepatterned acetylcholine receptor clusters in embryonic zebrafish skeletal muscle. J Neurosci. 2006; 26:934–47. [PubMed: 16421313]
8. Liu Y, et al. Essential roles of the acetylcholine receptor {gamma}-subunit in neuromuscular synaptic patterning. Development. 2008; 135:1957–67. [PubMed: 18434415]
9. Misgeld T, Kummer TT, Lichtman JW, Sanes JR. Agrin promotes synaptic differentiation by counteracting an inhibitory effect of neurotransmitter. Proc Natl Acad Sci U S A. 2005; 102:11088–93. [PubMed: 16043708]
10. Lin W, et al. Neurotransmitter acetylcholine negatively regulates neuromuscular synapse formation by a Cdk5-dependent mechanism. Neuron. 2005; 46:569–79. [PubMed: 15944126]
11. Fischbach GD, Nameroff M, Nelson PG. Electrical properties of chick skeletal muscle fibers developing in cell culture. J Cell Physiol. 1971; 78:289–99. [PubMed: 5167851]
12. Cohen SA, Fischbach GD. Regulation of muscle acetylcholine sensitivity by muscle activity in cell culture. Science. 1973; 181:76–8. [PubMed: 4736607]
13. Spector I, Prives JM. Development of electrophysiological and biochemical membrane properties during differentiation of embryonic skeletal muscle in culture. Proc Natl Acad Sci U S A. 1977; 74:5166–70. [PubMed: 270755]
14. Franzini-Armstrong C, Jorgensen AO. Structure and development of E-C coupling units in skeletal muscle. Annu Rev Physiol. 1994; 56:509–34. [PubMed: 8010750]
15. Tsien RW, Ellinor PT, Horne WA. Molecular diversity of voltage-dependent Ca2+ channels. Trends Pharmacol Sci. 1991; 12:349–54. [PubMed: 1659003]
16. Gregg RG, et al. Absence of the beta subunit (cchb1) of the skeletal muscle dihydropyridine receptor alters expression of the alpha 1 subunit and eliminates excitation-contraction coupling. Proc Natl Acad Sci U S A. 1996; 93:13961–6. [PubMed: 8943043]
17. Takeshima H, et al. Excitation-contraction uncoupling and muscular degeneration in mice lacking functional skeletal muscle ryanodine-receptor gene. Nature. 1994; 369:556–9. [PubMed: 7515481]
18. Nakai J, et al. Enhanced dihydropyridine receptor channel activity in the presence of ryanodine receptor. Nature. 1996; 380:72–5. [PubMed: 8598910]
19. Barone V, et al. Contractile impairment and structural alterations of skeletal muscles from knockout mice lacking type 1 and type 3 ryanodine receptors. FEBS Lett. 1998; 422:160–4. [PubMed: 9489997]
20. Sanes JR, Lichtman JW. Induction, assembly, maturation and maintenance of a postsynaptic apparatus. Nat Rev Neurosci. 2001; 2:791–805. [PubMed: 11715056]
21. Arikkath J, Campbell KP. Auxiliary subunits: essential components of the voltage-gated calcium channel complex. Curr Opin Neurobiol. 2003; 13:298–307. [PubMed: 12850214]

22. Ball SL, et al. Role of the beta(2) subunit of voltage-dependent calcium channels in the retinal outer plexiform layer. Invest Ophthalmol Vis Sci. 2002; 43:1595–603. [PubMed: 11980879]
23. Beurg M, et al. Recovery of Ca2+ current, charge movements, and Ca2+ transients in myotubes deficient in dihydropyridine receptor beta 1 subunit transfected with beta 1 cDNA. Biophys J. 1997; 73:807–18. [PubMed: 9251797]
24. Coronado R, Morrissette J, Sukhareva M, Vaughan DM. Structure and function of ryanodine receptors. Am J Physiol. 1994; 266:C1485–504. [PubMed: 8023884]
25. Bertocchini F, et al. Requirement for the ryanodine receptor type 3 for efficient contraction in neonatal skeletal muscles. Embo J. 1997; 16:6956–63. [PubMed: 9384575]
26. Duclert A, Changeux JP. Acetylcholine receptor gene expression at the developing neuromuscular junction. Physiol Rev. 1995; 75:339–68. [PubMed: 7724666]
27. Blau HM, Chiu CP, Webster C. Cytoplasmic activation of human nuclear genes in stable heterocaryons. Cell. 1983; 32:1171–80. [PubMed: 6839359]
28. Lee KS, Tsien RW. Mechanism of calcium channel blockade by verapamil, D600, diltiazem and nitrendipine in single dialysed heart cells. Nature. 1983; 302:790–4. [PubMed: 6302512]
29. Ahern CA, et al. Ca2+ current and charge movements in skeletal myotubes promoted by the beta-subunit of the dihydropyridine receptor in the absence of ryanodine receptor type 1. Biophys J. 2003; 84:942–59. [PubMed: 12547776]
30. Strube C, Beurg M, Powers PA, Gregg RG, Coronado R. Reduced Ca2+ current, charge movement, and absence of Ca2+ transients in skeletal muscle deficient in dihydropyridine receptor beta 1 subunit. Biophys J. 1996; 71:2531–43. [PubMed: 8913592]
31. Jorgensen AO, Shen AC, Arnold W, Leung AT, Campbell KP. Subcellular distribution of the 1,4-dihydropyridine receptor in rabbit skeletal muscle in situ: an immunofluorescence and immunocolloidal gold-labeling study. J Cell Biol. 1989; 109:135–47. [PubMed: 2545725]
32. Gomez-Ospina N, Tsuruta F, Barreto-Chang O, Hu L, Dolmetsch R. The C terminus of the L-type voltage-gated calcium channel Ca(V)1.2 encodes a transcription factor. Cell. 2006; 127:591–606. [PubMed: 17081980]
33. Schroder E, Byse M, Satin J. L-type calcium channel C terminus autoregulates transcription. Circ Res. 2009; 104:1373–81. [PubMed: 19461046]
34. Zhang Y, et al. The beta subunit of voltage-gated Ca2+ channels interacts with and regulates the activity of a novel isoform of Pax6. J Biol Chem. 2010; 285:2527–36. [PubMed: 19917615]
35. Pai AC. Developmental Genetics of a Lethal Mutation, Muscular Dysgenesis (Mdg), in the Mouse. I. Genetic Analysis and Gross Morphology. Dev Biol. 1965; 11:82–92. [PubMed: 14300095]
36. Pai AC. Developmental Genetics of a Lethal Mutation, Muscular Dysgenesis (Mdg), in the Mouse. Ii. Developmental Analysis. Dev Biol. 1965; 11:93–109. [PubMed: 14300096]
37. Powell JA, Rieger F, Blondet B, Dreyfus P, Pincon-Raymond M. Distribution and quantification of ACh receptors and innervation in diaphragm muscle of normal and mdg mouse embryos. Dev Biol. 1984; 101:168–80. [PubMed: 6692971]
38. Knudson CM, et al. Specific absence of the alpha 1 subunit of the dihydropyridine receptor in mice with muscular dysgenesis. J Biol Chem. 1989; 264:1345–8. [PubMed: 2536362]
39. Koenig J, Bournaud R, Powell JA, Rieger F. Appearance of contractile activity in muscular dysgenesis (mdg/mdg) mouse myotubes during coculture with normal spinal cord cells. Dev Biol. 1982; 92:188–96. [PubMed: 7106378]
40. Rieger F, et al. Restoration of dysgenic muscle contraction and calcium channel function by co-culture with normal spinal cord neurons. Nature. 1987; 330:563–6. [PubMed: 2446145]
41. Lomo T, Rosenthal J. Control of ACh sensitivity by muscle activity in the rat. J Physiol. 1972; 221:493–513. [PubMed: 4336524]
42. Witzemann V, Brenner HR, Sakmann B. Neural factors regulate AChR subunit mRNAs at rat neuromuscular synapses. J Cell Biol. 1991; 114:125–41. [PubMed: 1646821]
43. Valenzuela DM, et al. Receptor tyrosine kinase specific for the skeletal muscle lineage: expression in embryonic muscle, at the neuromuscular junction, and after injury. Neuron. 1995; 15:573–84. [PubMed: 7546737]

44. Lomo T, Westgaard RH. Further studies on the control of ACh sensitivity by muscle activity in the rat. J Physiol. 1975; 252:603–26. [PubMed: 1206569]
45. Mejat A, et al. Histone deacetylase 9 couples neuronal activity to muscle chromatin acetylation and gene expression. Nat Neurosci. 2005; 8:313–21. [PubMed: 15711539]
46. Tang H, et al. A histone deacetylase 4/myogenin positive feedback loop coordinates denervation-dependent gene induction and suppression. Mol Biol Cell. 2009; 20:1120–31. [PubMed: 19109424]
47. Rotzler S, Schramek H, Brenner HR. Metabolic stabilization of endplate acetylcholine receptors regulated by Ca2+ influx associated with muscle activity. Nature. 1991; 349:337–9. [PubMed: 1846230]
48. Deisseroth K, Mermelstein PG, Xia H, Tsien RW. Signaling from synapse to nucleus: the logic behind the mechanisms. Curr Opin Neurobiol. 2003; 13:354–65. [PubMed: 12850221]
49. West AE, Griffith EC, Greenberg ME. Regulation of transcription factors by neuronal activity. Nat Rev Neurosci. 2002; 3:921–31. [PubMed: 12461549]
50. Arber S, et al. Requirement for the homeobox gene Hb9 in the consolidation of motor neuron identity. Neuron. 1999; 23:659–74. [PubMed: 10482234]

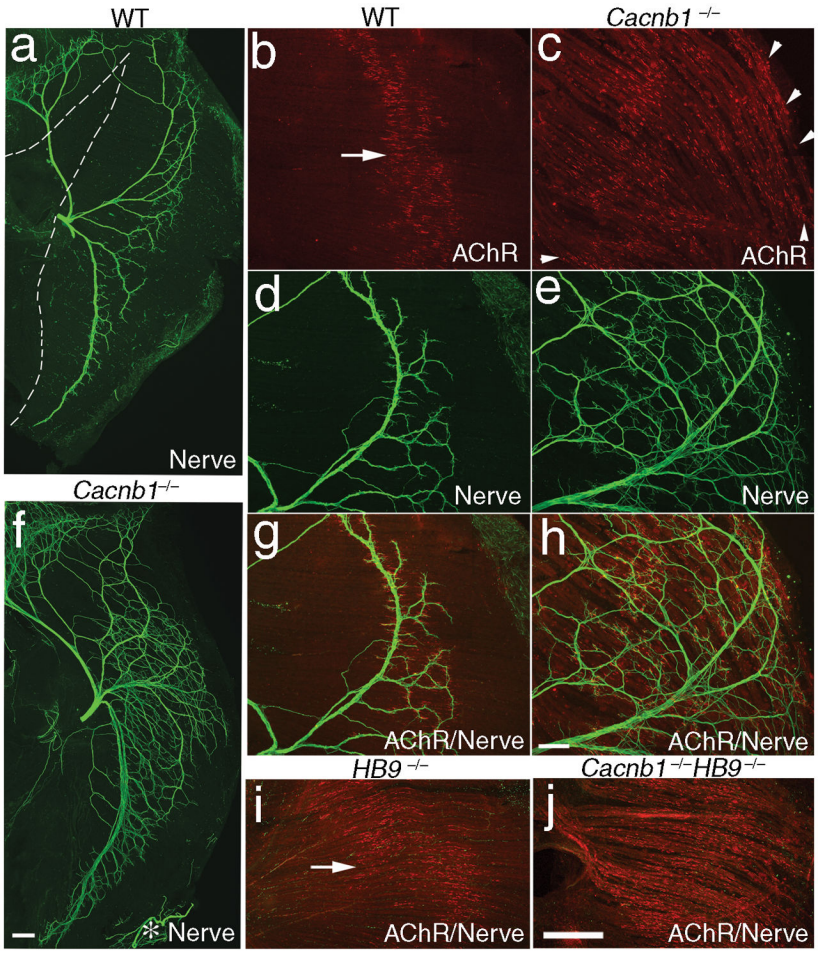

Figure 1. Loss of DHPR function leads to defects in muscle pre-patterning

Whole mounts of diaphragm muscles (E14.5) were double-labeled by α-bgt for AChR and by anti-neurofilament (NF150) and anti-synaptotagmin 2 (Syt2) for the nerve. Increased nerve branching and expansion of innervation territories were detected in *Cacnb1*$^{-/-}$ muscle (**f**) compared with WT muscle (**a**). White dashed lines (**a)** delineate the myotendinous junction between the central tendon and the medial edge of the muscle fibers. The asterisk (*) (**f**) indicates a small branch of the intercostal nerve attached to the outer edge of the diaphragm muscle. **b–e, g–h**: high-magnification views of the dorsal regions of the diaphragm muscle. In the WT muscle, AChR clusters were aligned along the central region of the muscle, forming a pre-patterned end-plate band (arrow in **b**); the nerves extend fine branches and terminate within the central end-plate band (**d, g**). In contrast, in the *Cacnb1*$^{-/-}$ muscle, AChR clusters were distributed broadly across the entire surface of the muscle, including the medial and lateral edges of the muscle (arrowheads in **c**); the nerves in the *Cacnb1*$^{-/-}$ muscle also branched extensively and expanded their innervation territories across the entire muscle surface (**e, h**). At this stage, the majority of the AChR clusters were not directly apposed to the nerve terminal (**g**, **h**). **i–j**: AChR clusters were distributed along a central end-plate band in *HB9*$^{-/-}$ muscles (**i**), but were distributed broadly in double null *Cacnb1*$^{-/-}$ *HB9*$^{-/-}$ muscles (**j**). Scale bar: a, f: 200 μm; b–e, g–h: 100 μm; i–j: 400 μm.

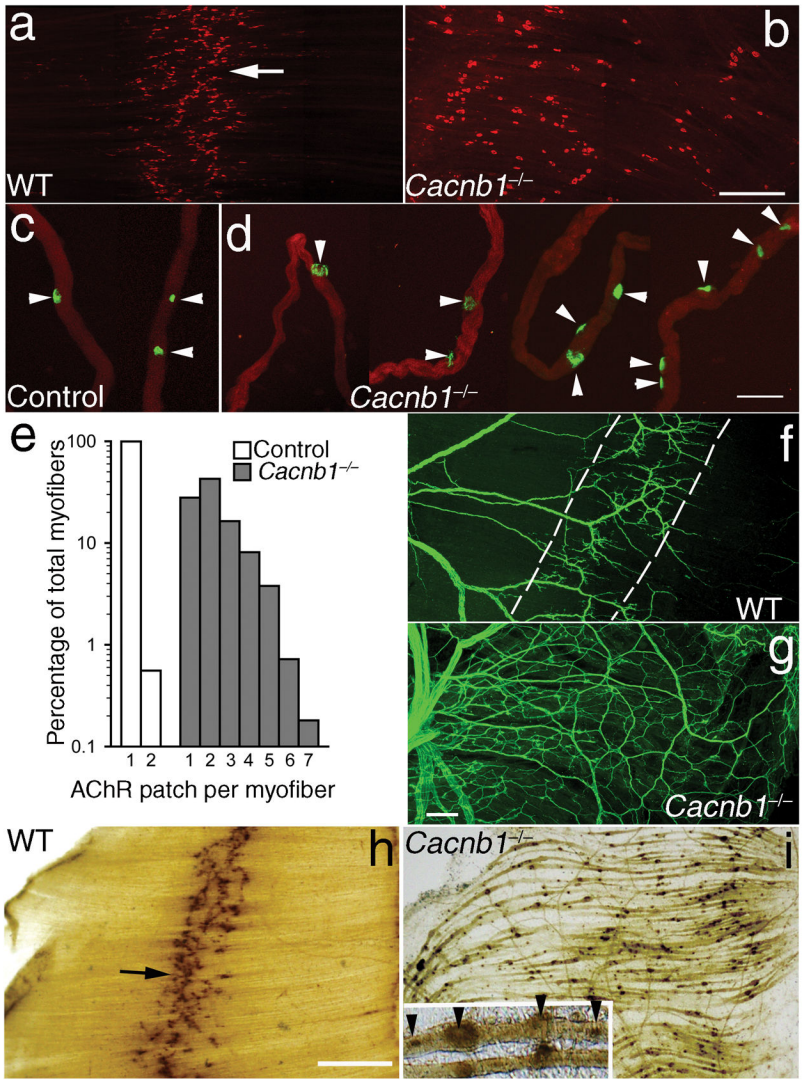

Figure 2. Loss of DHPR function leads to multiple synaptic sites and an expansion of innervation territories

a–b: Distribution of AChR clusters (labeled by α-bgt) in whole mounts of diaphragm muscles (E18.5). AChR clusters were aligned in a central endplate band in WT (arrow in **a**), but were scattered over a broad region in *Cacnb1*$^{-/-}$ muscles (**b**). **c-d**: Dissociated myofibers stained with FITC-conjugated α-bgt and rhodamine-conjugated phalloidin. **e**: histogram distribution of the percentage (in log scale) of dissociated myofibers containing various numbers of endplates ranging from 1 to 7. Multiple endplates were frequently detected in dissociated *Cacnb1*$^{-/-}$ myofibers (**d**); the majority of them (72%, 399 out of 554) contained 2 or more endplates per fiber (2 patches: 42.8%; 3 patches: 16.4%; 4 patches: 8.1%; 5 patches: 3.8%; 6 patches: 0.7% and 7 patches: 0.2%). In contrast, the majority of control myofibers (99.4%, 357 out of 359) contained single endplate; less than 1% of them (0.6%, 2 out of 359) contained two endplates per fiber. **f–g**: The innervation territories were confined within the central region in the WT (bordered by dashed lines **f**), but expanded to the entire muscle in *Cacnb1*$^{-/-}$ (**g**). **h–i**: Distribution of AChE clusters (arrow) revealed by

cholinesterase staining. AChE clusters were localized along the central region of the muscle in the WT (**h**), but were broadly distributed in the *Cacnb1*$^{-/-}$ muscle (**i**). Inset in **i** shows a high power view of individual myofibers containing multiple AChE clusters (arrowheads) in *Cacnb1*$^{-/-}$ muscle. Scale bars: a–b: 400 μm; c–d: 50 μm; f–g: 200 μm; h–i: 250 μm.

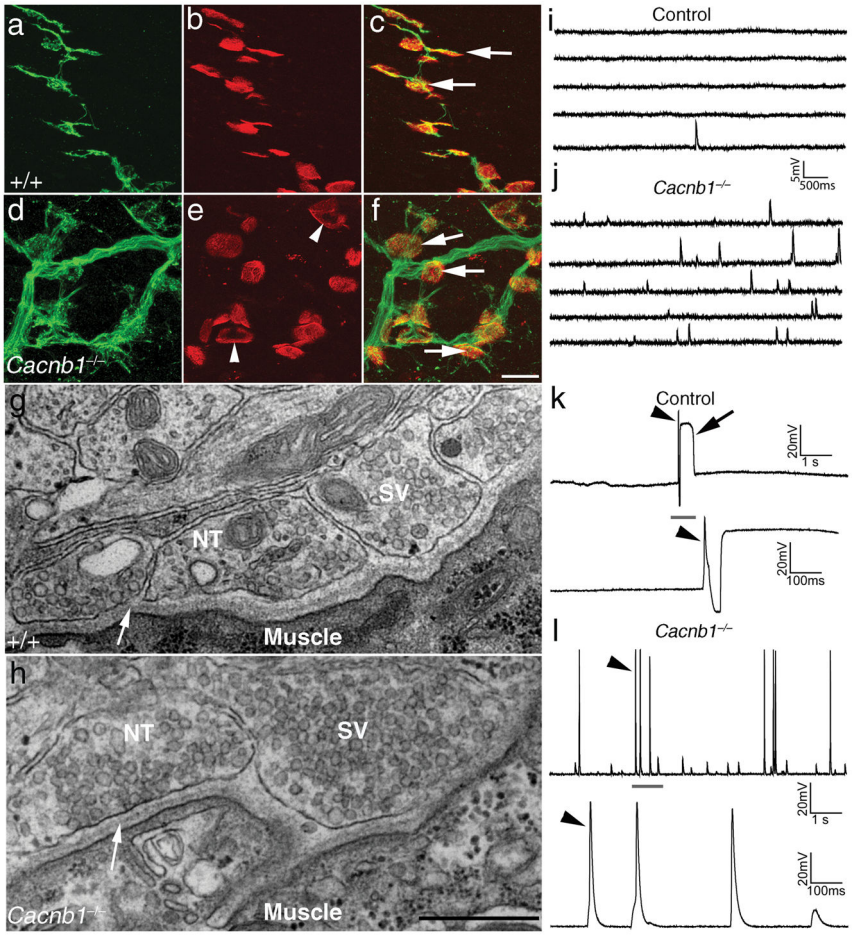

Figure 3. DHPR function is not required for synaptogenesis, but its absence leads to increased synaptic and muscle electrical activity

a–f: Confocal images of E18.5 diaphragm muscles doubly labeled by presynaptic markers (NF150 and Syt2) (**a**, **d**) and postsynaptic marker α-bgt (**b**, **e**). Every end-plate in both WT (**b**) and the *Cacnb1*$^{-/-}$ muscle (**e**) was fully innervated by the nerves (arrows in **c**, **f**). Endplates in the control muscle appeared predominantly as ovoid-shaped plaques (**b**), whereas endplates in *Cacnb1*$^{-/-}$ muscles were bigger, and some were perforated (arrowheads in **e**). **g-h**: Electron micrographs of the NMJ (E18.5, diaphragm muscle). In both WT (**g**) and *Cacnb1*$^{-/-}$ (**h**), synaptic vesicles (SV) were abundantly present at the nerve terminal (NT), and the basal lamina (white arrow in **g**, **h**) was well-defined in the synaptic cleft. **i–j**: Sample traces of mEPPs from control (**i**) and *Cacnb1*$^{-/-}$ (**j**) myofibers. The mEPP frequency was markedly increased in *Cacnb1*$^{-/-}$ muscles. **k–l**: Spontaneous action potentials (arrowheads) in control (**k**) and *Cacnb1*$^{-/-}$ (**l**) mice; the lower trace in **k** and **l** illustrates an expanded view of the portion of the upper trace indicated by the grey line. Arrow in **k** indicates the displacement of the trace resulting from muscle contraction in the control. Scale bars: a–f: 20 μm; g–h: 0.5 μm.

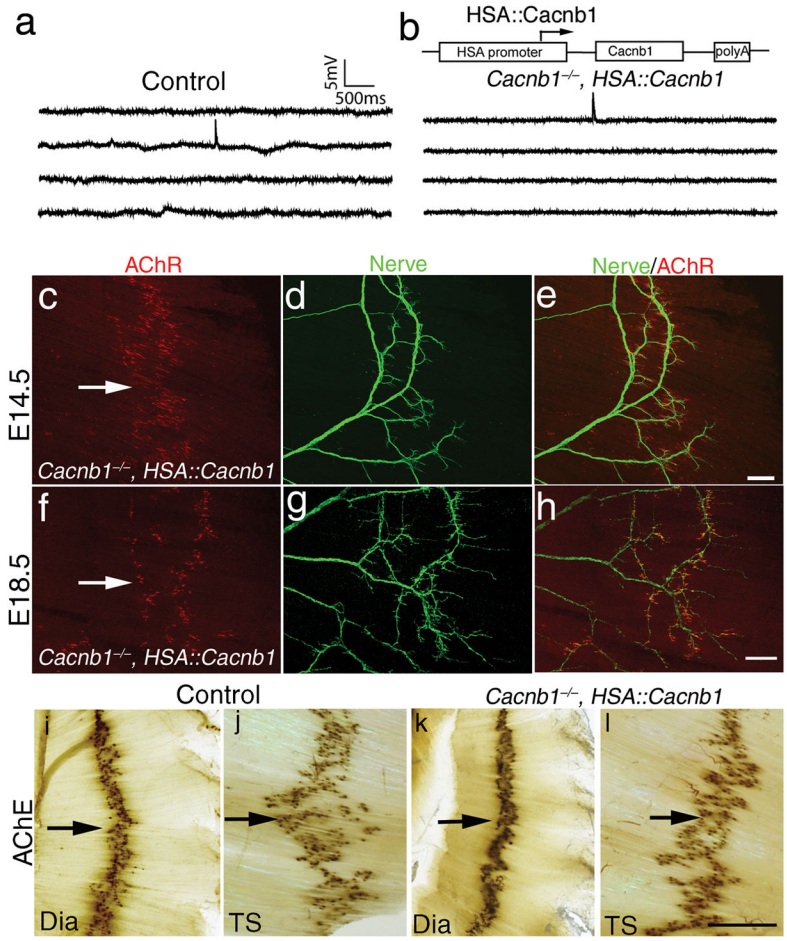

Figure 4. Muscle-specific expression of *Cacnb1* rescues the patterning defects in *Cacnb1*$^{-/-}$ muscle

a–b: Sample traces of mEPP recorded from P0 diaphragm muscles in control (**a**) and the *Cacnb1*$^{-/-}$ mice that also carry a *HSA::Cacnb1* transgene under the control of the muscle-specific HSA promoter, as shown in the schematic drawing [*Cacnb1*$^{-/-}$*; HSA::Cacnb1*, referred to as the rescued mice (**b**)]. **c–h**: Wholemount diaphragm muscles at E14.5 (**c–e**) and E18.5 (**f–h**) from the rescued mice (*Cacnb1*$^{-/-}$*; HAS::Cacnb1)* were double-labeled for AChRs (**c, f**) and the nerves (**d, g**). Similar to the WT muscles (compared to Fig. 1, Fig. 2), AChR clusters in the rescued muscles were aligned to a central endplate band (arrow in **c, f**) and nerve terminals were also confined to a central endplate band as shown in the merged images (**e, h). i–l**: AChE staining of wholemount diaphragm muscle (Dia, P0) and triangularis sterni muscle (TS, P90) from control (**i**, **j**) and the rescued mice (*Cacnb1*$^{-/-}$*; HAS::Cacnb1)* (**k**, **l**). The patterns of AChE staining (black arrow) were similar between control and the rescued mice. Scale bars: c–e, 100 μm, f–h, 200 μm; i–l, 1000 μm.

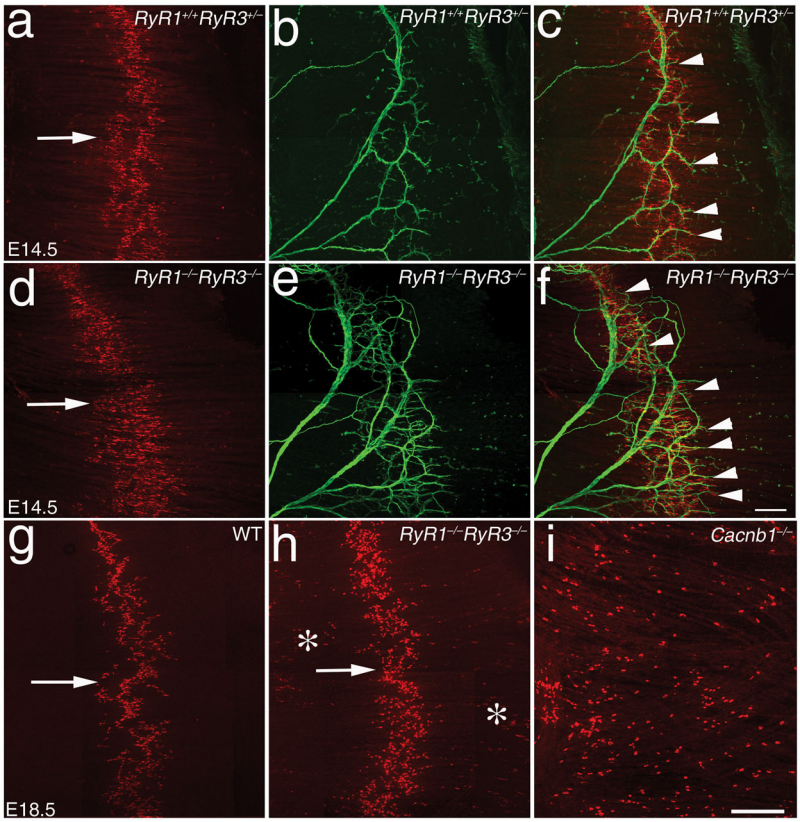

Figure 5. RyRs and DHPRs play different roles in muscle pre-patterning

a–f: Distribution of AChR clusters (**a**, **d**), nerves (**b**, **e**) and merged images (**c**, **f**) revealed by double-immunofluroscence staining of E14.5 diaphragm muscles from *RyR1*$^{-/-}$*RyR3*$^{-/-}$ (**d–f**) and littermate control mice (*RyR1*$^{+/+}$*RyR3*$^{+/-}$, **a–c**). AChRs were clustered along central regions of the muscles in both *RyR1*$^{-/-}$*RyR3*$^{-/-}$ and *RyR1*$^{+/+}$*RyR3*$^{+/-}$ mice (arrows in **a**, **d**), in a pattern similar to that seen in the WT mice (Fig. 1b). Increased innervation was detected in *RyR1*$^{-/-}$*RyR3*$^{-/-}$ (**e**) compared with the control (*RyR1*$^{+/+}$*RyR3*$^{+/-}$, **b)**. Nevertheless, nerve terminals in both *RyR1*$^{-/-}$*RyR3*$^{-/-}$ and *RyR1*$^{+/+}$*RyR3*$^{+/-}$ mice were confined to the central region of the muscle as shown in the merged images (arrowheads in **c**, **f**). **g–i**: AChR distribution in E18.5 diaphragm muscles. Unlike *Cacnb1*$^{-/-}$ muscle in which AChR clusters were broadly distributed (**i),** the majority of AChR clusters were aligned in a central end-plate band in E18.5 *RyR1*$^{-/-}$*RyR3*$^{-/-}$ muscle (arrow in **h**), similar to the end-plate band seen in the E18.5 WT muscle (arrow in **g**). However, some AChR clusters were ectopically localized to the peripheral regions of the E18.5 *RyR1*$^{-/-}$*RyR3*$^{-/-}$ muscle (* in **h**). Scale bar: **a–f**: 100 μm; **g–i**: 400 μm.

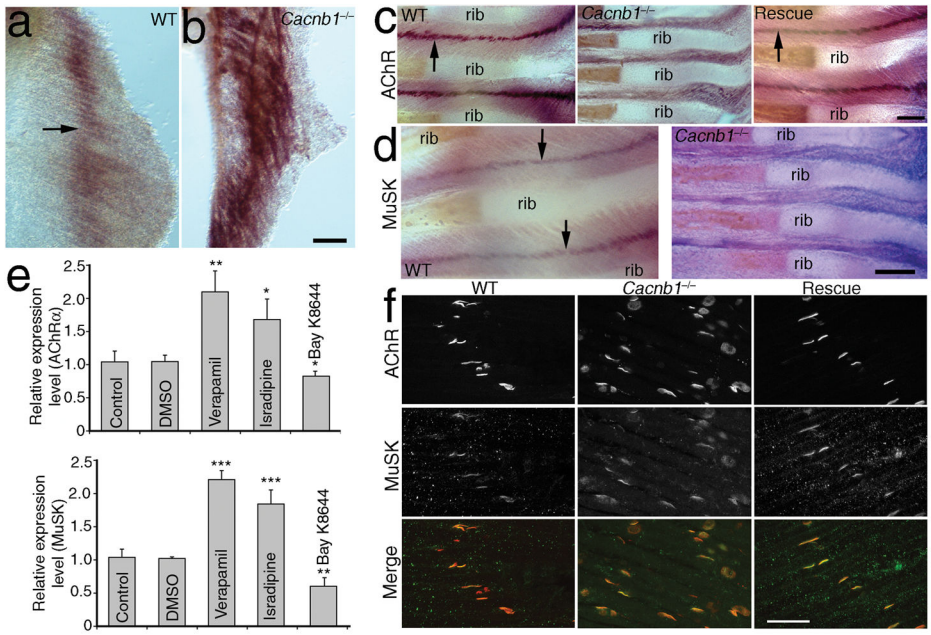

Figure 6. DHPRs pattern neuromuscular synapses by regulating the expression of *AChR* and *MuSK*

Wholemount in situ hybridization with DIG-labeled *AChRα* probes were carried out in E14.5 diaphragm muscles (**a–b**) or E18.5 intercostal muscles (**c**). *AChRα* transcripts were detected along the central regions in the WT (**a**), but were broadly distributed in the *Cacnb1*$^{-/-}$ muscle (**b**). **c**: *AChRα* transcripts were localized to the central region of the WT muscle (left panel in **c**), but were detected in the entire *Cacnb1*$^{-/-}$ muscle (middle panel in **c**). The normal distribution of *AChRα* transcripts was restored in the rescued mice (right panel in **c**). **d**: Wholemount in situ hybridization of intercostal muscles using DIG-labeled *MuSK* probes. *MuSK* transcripts were localized to the central region of the WT (left), but were broadly distributed in the *Cacnb1*$^{-/-}$ muscle (right)**. e**: Relative expression levels of AChR and MuSK assayed by quantitative real-time PCR in C2C12 myotube cultures treated with L-type Ca^{2+} channel antagonists (verapamil, isradipine) or agonist (Bay K 8644) compared to the untreated or vehicle (DMSO) treated controls. Verapamil (10 μM) significantly increased the relative expression levels of *MuSK* (2.21 ± 0.13, N = 5 cultures, *P* = 0.0002) and *AChR* (2.10 ± 0.32, N = 5 cultures, *P* = 0.009) compared with controls (*MuSK*, 1.03 ± 0.12; *AChR*, 1.04 ± 0.16, N = 5 cultures). Similarly, isradipine (1 μM) also significantly increased the relative expression levels of *MuSK* (1.84 ± 0.21, N = 3 cultures, *P* = 0.0003) and *AChR* (1.68 ± 0.31, N = 3 cultures, *P* = 0.0189) compared with controls (*MuSK*, 1.01 ± 0.10; *AChR*, 1.00 ± 0.02, N = 3 cultures). Bay K 8644 significantly decreased the expression of *MuSK* (0.60 ± 0.13, N = 3 cultures, *P* = 0.0012) and *AChR* (0.83 ± 0.07, N = 3 cultures, *P* = 0.0337) compared with controls (*MuSK*, 1.02 ± 0.02; *AChR*, 1.04 ± 0.10, N = 6 cultures). **f:** Wholemount diaphragm muscles were immunostained with anti-MuSK antibodies and α-bgt. MuSK protein was clustered along the central region of the WT (left column), but broadly distributed in the *Cacnb1*$^{-/-}$ muscles (middle column). MuSK

distribution was restored to normal in the rescued mice (right column). Data are presented as mean ± SEM. Scale bars: a–b: 500 μm; c: 500 μm; d: 400 μm; f: 50 μm.